Chapter 11

Pre-supernova evolution of massive stars

We have seen that low- and intermediate-mass stars (with masses up to $\approx 8\,M_\odot$) develop carbon-oxygen cores that become degenerate after central He burning. As a consequence the maximum core temperature reached is smaller than required for carbon fusion. During the latest stages of evolution on the AGB these stars undergo strong mass loss which removes the remaining envelope, so that their final remnants are C-O white dwarfs.

The evolution of *massive stars* is different in two important ways:

- They reach a sufficiently high temperature in their cores (5×10^8 K) to undergo *non-degenerate carbon ignition* (see Fig. 11.1). This requires a certain minimum mass for the CO core after central He burning, which detailed evolution models put at $M_{\mathrm{CO-core}} > 1.06\,M_\odot$. Only stars with (initial) masses above a certain limit, often denoted as M_{up} in the literature, reach this critical core mass. The value of M_{up} is somewhat uncertain, mainly due to uncertainties related to mixing (e.g. convective overshooting), but is approximately $8\,M_\odot$.

  Stars with masses above the limit $M_{\mathrm{ec}} \approx 11\,M_\odot$ also ignite and burn fuels heavier than carbon until an Fe core is formed which collapses and causes a supernova explosion.[1] We will explore the evolution of the cores of massive stars through carbon burning, up to the formation of an iron core, in the second part of this chapter.

- For masses $M \gtrsim 15\,M_\odot$, *mass loss by stellar winds* becomes important during all evolution phases, including the main sequence. For masses above $30\,M_\odot$ the mass-loss rates $\dot{M}$ are so large that the timescale for mass loss, $\tau_{\mathrm{ml}} = M/\dot{M}$, becomes smaller than the nuclear timescale τ_{nuc}. Therefore mass loss has a very significant effect on their evolution. The stellar wind mechanisms involved are in many cases not well understood, so that $\dot{M}$ is often quite uncertain. This introduces substantial uncertainties in massive star evolution. The effect of mass loss on massive star evolution is discussed in the first part of this chapter.

11.1 Stellar wind mass loss

Observations in the ultraviolet and infrared part of the spectrum show that luminous stars, with masses above about $15\,M_\odot$, undergo rapid mass outflows (stellar winds) that gradually erode their outer lay-

[1] The fate of stars in the approximate mass range $8 - 11\,M_\odot$ is still somewhat uncertain. They develop degenerate O-Ne cores after central C-burning, and their structure is then very similar to those of AGB stars with degenerate CO cores. Such stars have been named *super-AGB* stars in recent years.

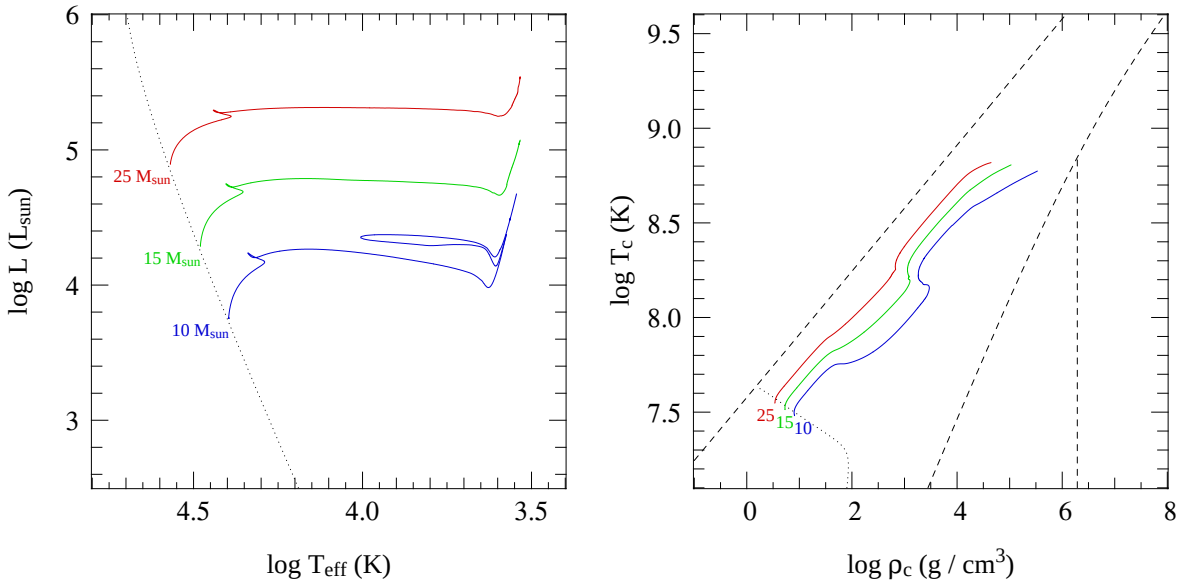

Figure 11.1. Evolution tracks in the HR diagram (left panel) and in the $\log\rho_c$-$\log T_c$ diagram (right panel) for stars with $Z = 0.02$ and $M = 10$, 15 and 25 $M_\odot$, computed with a moderate amount of overshooting. The tracks end when carbon is ignited in the centre, under non-degenerate conditions.

ers. An empirical formula that fits the average observed mass-loss rates of stars in the upper part of the HR diagram ($L \gtrsim 10^3\,L_\odot$) was derived by De Jager and others in 1988:

$$\log(-\dot{M}) \approx -8.16 + 1.77\log\left(\frac{L}{L_\odot}\right) - 1.68\log\left(\frac{T_{\rm eff}}{\rm K}\right) \qquad \text{(in } M_\odot\text{/yr)}. \tag{11.1}$$

For example, for the 25 $M_\odot$ star depicted in Fig. 11.1 you can check by estimating L and $T_{\rm eff}$ from the graph that this implies a mass loss of $5\times10^{-8}\,M_\odot$/yr at the ZAMS, increasing up to $5\times10^{-7}\,M_\odot$/yr at the end of the main sequence. By the end of the evolution track, when the star is a red supergiant, the mass-loss rate implied by the above formula has increased to $5\times10^{-5}\,M_\odot$/yr.

The observed strong mass loss is probably caused by different mechanisms in different parts of the HR diagram.

Radiation-driven stellar winds

Hot, luminous stars (OB-type main-sequence stars and *blue supergiants*, BSG) undergo a fast *radiation-driven stellar wind*. Radiation pressure at frequencies corresponding to absorption lines in the spectrum, where the interaction between photons and matter is strong, causes an outward acceleration. An upper limit to the mass-loss rate that can be driven by radiation is obtained by assuming that the photons transfer their entire momentum to the outflowing matter:

$$\dot{M}v_\infty < \frac{L}{c} \tag{11.2}$$

where v_∞ is the terminal wind velocity at large distance from the star ('infinity'). A typical value of the terminal velocity is about three times the escape velocity, $v_\infty \approx 3v_{\rm esc}$ (about 1000–3000 km/s for O-type stars). Comparing the mass-loss rates from eq. (11.1) with the upper limit shows that the empirical rates are indeed smaller, but only by a factor 1/3 to 1/6: apparently momentum is transferred quite efficiently from the photons to the wind. This can be attributed to the acceleration of the wind: the associated Doppler broadening of the spectral lines means a large part of the flux can be used (the

outflowing atoms can absorb photons of a different, higher frequency as they get accelerated). This is a positive feedback mechanism that reinforces the wind driving.

The theory for radiation-driven winds is quite well developed, but the theoretical predictions for $\dot{M}$ are uncertain due to inhomogeneities in the wind ('clumping'). The uncertain clumping factor also affects the mass-loss rates inferred from observations, and current estimates are typically a factor ~ 3 lower than the the empirical rate of eq. (11.1). Radiation-driven mass loss is also dependent on metallicity, because it is mostly the lines of the heavier elements that contribute to the line driving. A dependence $\dot{M} \propto Z^{0.7}$ has been inferred theoretically, as well as from observations.

Red supergiant mass loss

Cool, luminous stars known as *red supergiants* (RSG) undergo a slow but copious stellar wind that is probably driven by the same mechanism as the 'superwind' of AGB stars: a combination of stellar pulsations and radiation pressure on dust particles that form in the cool outer atmosphere. There are no theoretical predictions, so we must rely on observations which imply very high values of $\dot{M}$ up to $10^{-4} M_\odot$/yr (eq. 11.1).

Stars with $M \lesssim 40\,M_\odot$ spend a large fraction of their *core He-burning* phase as red supergiants. During this phase a large part or even the entire envelope can be evaporated by the wind, exposing the helium core of the star as a Wolf-Rayet (WR) star (see Sect. 11.1.2).

11.1.1 The Humphreys-Davidson limit and luminous blue variables

Observations of the most luminous stars in our Galaxy and in the Magellanic Clouds have revealed a clear upper limit to stellar luminosities that depends on the effective temperature (see Fig. 11.2). In particular there are no red supergiants in HR diagram with $\log(L/L_\odot) > 5.8$, which corresponds to the expected RSG luminosity of a star of $40\,M_\odot$. Apparently stars with $M \gtrsim 40\,M_\odot$ do not become red supergiants.

The upper limit in the HRD is known as the *Humphreys-Davidson limit* after its discoverers, Roberta Humphreys and Kris Davidson. At $T_{\rm eff}$ above 10 000 K the maximum luminosity increases gradually to $\log(L/L_\odot) = 6.8$ at 40 000 K (O stars).

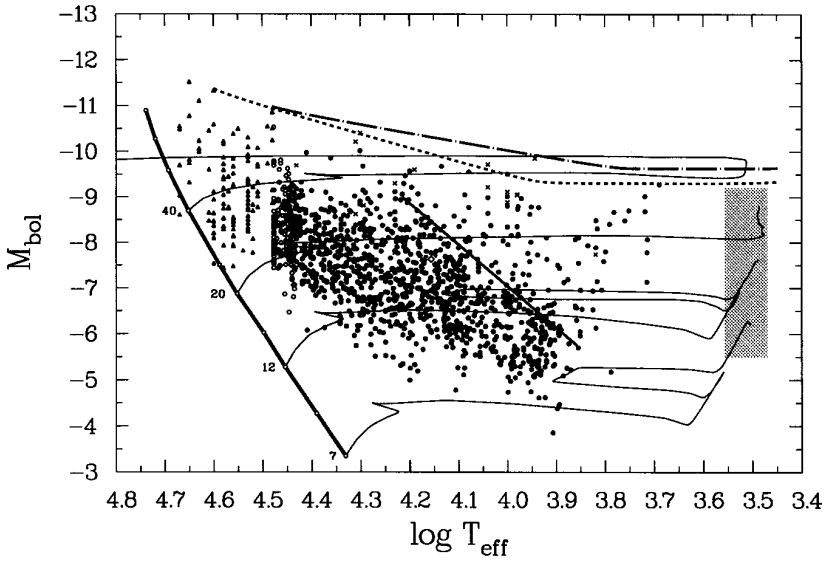

Figure 11.2. The HRD of the brightest supergiants in the LMC. The shaded region contains several hundred red supergiants that are not individually shown. The upper envelope of observed stars traced by the dotted line is known as the Humphreys-Davidson limit (the lower envelope is simply an observational cut-off). Figure from Fitzpatrick & Garmany (1990).

The existence of the HD limit is interpreted as a (generalized) Eddington limit. We have seen in Sec. 4.4 that when the luminosity of a star exceeds the classical Eddington limit (eq. 4.38),

$$L_{\rm Edd} = \frac{4\pi cGM}{\kappa}, \tag{11.3}$$

where κ is the electron-scattering opacity, the outward force due to radiation pressure on the free electrons exceeds the gravitational force (on the nuclei) inwards. The electrostatic coupling between electrons and ions means that the outer layers are accelerated outwards and the star becomes unstable. However, the *actual* opacity in the atmosphere is larger than the electron-scattering opacity, and decreases with temperature. Therefore the luminosity at which the radiation-pressure limit is reached is lower than the classical Eddington limit, and the decrease of the HD limit with decreasing $T_{\rm eff}$ can be explained at least qualitatively by this effect.

Luminous stars located near the HD limit are indeed observed to be very unstable, undergoing large excursions in the HRD and episodic mass loss with $\dot{M} \gtrsim 10^{-3}\,M_\odot$/yr during outbursts. These stars are known as *luminous blue variables* (LBVs), examples of which in our Galaxy are η Carinae and P Cygni. The remnants of the vigorous mass loss episodes are seen as circumstellar nebulae, which in the extreme case of η Car contains $\sim 10\,M_\odot$ ejected during an outburst in the mid-1800s. The nebula is considerably enriched in nitrogen, showing that the layers processed by CNO-cycling are being ejected. Stars losing mass due to LBV outbursts are destined to become *Wolf-Rayet stars*. The strong LBV mass loss prevents them from ever becoming red supergiants.

11.1.2 Wolf-Rayet stars

Wolf-Rayet (WR) stars are hot, very luminous stars with bright emission lines in their spectra. The emission indicates very strong, optically thick stellar winds, with mass-loss rates of $\dot{M} \sim 10^{-5} - 10^{-4}\,M_\odot$/yr. They are often surrounded by circumstellar nebulae of ejected material. The winds are probably driven by radiation pressure as for O stars, but multiple photon scattering in the optically thick outflow can increase the mass-loss rate to well above the single-scattering limit (eq. 11.2).

The spectra of WR stars reveal increased CNO abundances, indicating that they are the exposed H- or He-burning cores of massive stars. On the basis of the surface abundances they are classified into several subtypes:

WNL stars have hydrogen present on their surfaces (with $X_{\rm H} < 0.4$) and increased He and N abundances, consistent with equilibrium values from the CNO-cycle

WNE stars are similar to WNL stars in terms of their He and N abundances, but they lack hydrogen ($X_{\rm H} = 0$)

WC stars have no hydrogen, little or no N, and increased He, C and O abundances (consistent with partial He-burning)

WO stars are similar to WC stars with strongly increased O abundances (as expected for nearly complete He burning)

This apparently represents an *evolutionary sequence* of exposure of deeper and deeper layers, as a massive star is peeled off to a larger and larger extent by mass loss.

11.2 Evolution of massive stars with mass loss in the HR diagram

Fig. 11.3 shows evolution tracks in the HRD for massive stars calculated with mass loss at $Z = 0.02$. As revealed by this figure, the evolutionary journey of a massive star through the HRD can be rather

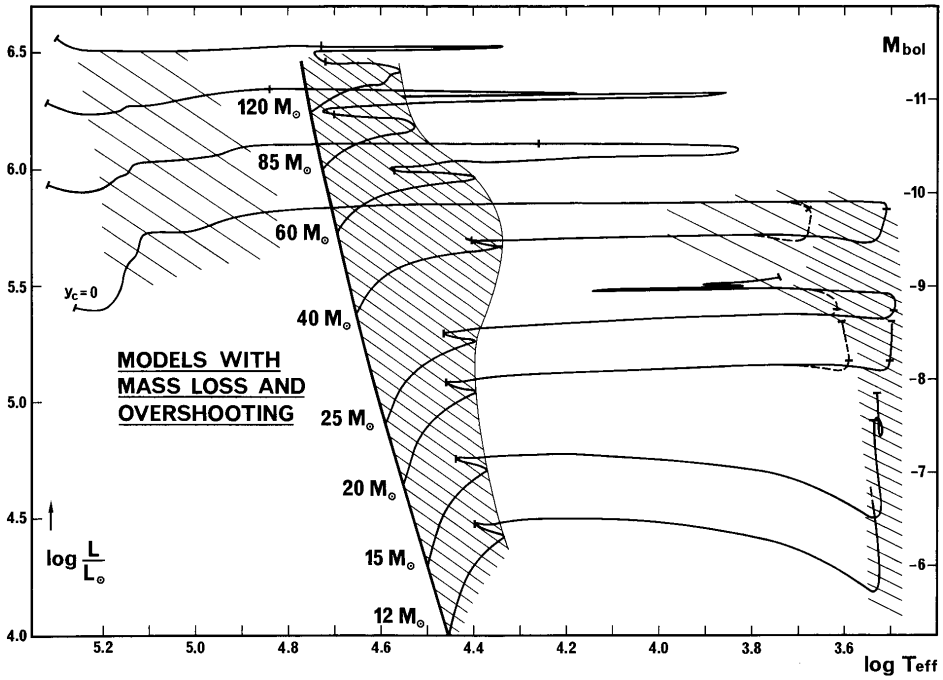

Figure 11.3. Evolution tracks of massive stars ($12 - 120\,M_\odot$) calculated with mass loss and a moderate amount of convective overshooting ($0.25\,H_P$). The shaded regions correspond to long-lived evolution phases on the main sequence, and during core He burning as a RSG (at $\log T_{\rm eff} < 4.0$) or as a WR star (at $\log T_{\rm eff} > 4.8$). Stars with initial mass $M > 40\,M_\odot$ are assumed to lose their entire envelope due to LBV episodes and never become RSGs. (Figure from Maeder & Meynet 1987).

complicated, showing several left-right excursions and loops which depend on the mass (by comparison, the evolution of the centre of the star is much simpler, see next sections). The relation between the theoretical evolution tracks and the zoo of observed types of massive star encountered in Sec. 11.1 is described by the following *evolution scenarios* for massive stars of Population I composition ($Z \sim 0.02$)[2] :

$M \lesssim 15\,M_\odot$	MS (OB) → RSG (→ BSG in blue loop? → RSG) → SN II mass loss is relatively unimportant, $\lesssim$ few $M_\odot$ is lost during entire evolution
$15\,M_\odot \lesssim M \lesssim 25\,M_\odot$	MS (O) → BSG → RSG → SN II mass loss is strong during the RSG phase, but not strong enough to remove the whole H-rich envelope
$25\,M_\odot \lesssim M \lesssim 40\,M_\odot$	MS (O) → BSG → RSG → WNL → WNE → WC → SN Ib the H-rich envelope is removed during the RSG stage, turning the star into a WR star
$M \gtrsim 40\,M_\odot$	MS (O) → BSG → LBV → WNL → WNE → WC → SN Ib/c an LBV phase blows off the envelope before the RSG can be reached

The last scenario is highlighted in Fig. 11.4 for a $60\,M_\odot$ star. After about 3.5 Myr, while the star is still on the main sequence, mass loss exposes layers that formerly belonged to the (large) convective core. Thus CNO-cycling products (nitrogen) are revealed, and the surface He abundance increases

[2]The relation of the final state to the supernova types indicated in this overview will be treated in Chapter 12.

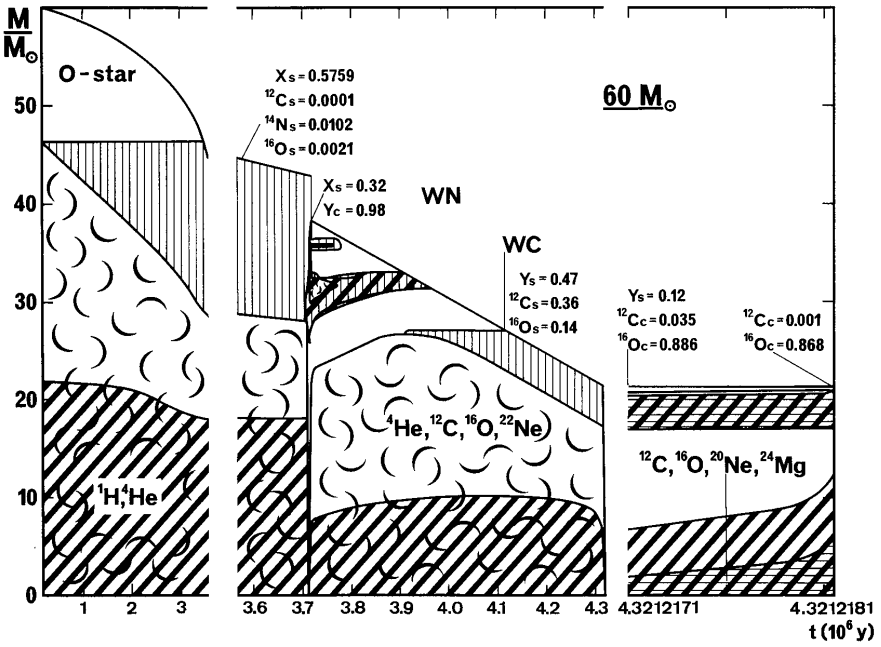

Figure 11.4. Kippenhahn diagram of the evolution of a $60\,M_\odot$ star at $Z = 0.02$ with mass loss. Cross-hatched areas indicate where nuclear burning occurs, and curly symbols indicate convective regions. See text for details. (Figure from Maeder & Meynet 1987).

at the expense of H. During the very short phase between central H and He burning ($t = 3.7$ Myr), several $M_\odot$ are rapidly lost in an LBV phase. During the first part of core He burning (3.7 – 3.9 Myr) the star appears as a WNL star, and subsequently as a WNE star (3.9 – 4.1 Myr) after mass loss has removed the last H-rich layers outside the H-burning shell. After 4.1 Myr material that was formerly in the He-burning convective core is exposed at the surface: N, which was consumed in He-burning reactions, disappears while the products of He-burning, C and O, appear. The last 0.2 Myr of evolution this star spends as a WC star.

In general, mass-loss rates during all evolution phases increase with stellar mass, resulting in timescales for mass loss that are less that the nuclear timescale for $M \gtrsim 30\,M_\odot$. As a result, there is a *convergence* of the final (pre-supernova) masses to $\sim 5 - 10\,M_\odot$. However, this effect is much diminished for metal-poor stars because the mass-loss rates are generally lower at low metallicity. The mass limits between the scenarios given above are therefore increase at lower metallicity.

11.3 Advanced evolution of massive stars

The evolution of the surface properties described in the previous section corresponds to the hydrogen and helium burning phases of massive stars. Once a carbon-oxygen core has formed after He burning, which is massive enough ($> 1.06\,M_\odot$) to undergo carbon ignition, the subsequent evolution of the *core* is a series of alternating nuclear burning and core contraction cycles in quick succession (see Fig. 11.5). Due to strong *neutrino losses* (see Sect. 11.3.1) the core evolution is sped up enormously: $\lesssim 10^3$ years pass between the onset of carbon burning until the formation of an iron core. During this time the mass of the C-O core remains fixed. Furthermore, the stellar *envelope* hardly has time to respond to the rapid changes in the core, with the consequence that the evolution of the envelope is practically disconnected from that of the core. As a result the position of a massive star in the HR diagram remains almost unchanged during carbon burning and beyond. We can thus concentrate on the evolution of the core of the star from this point onwards.

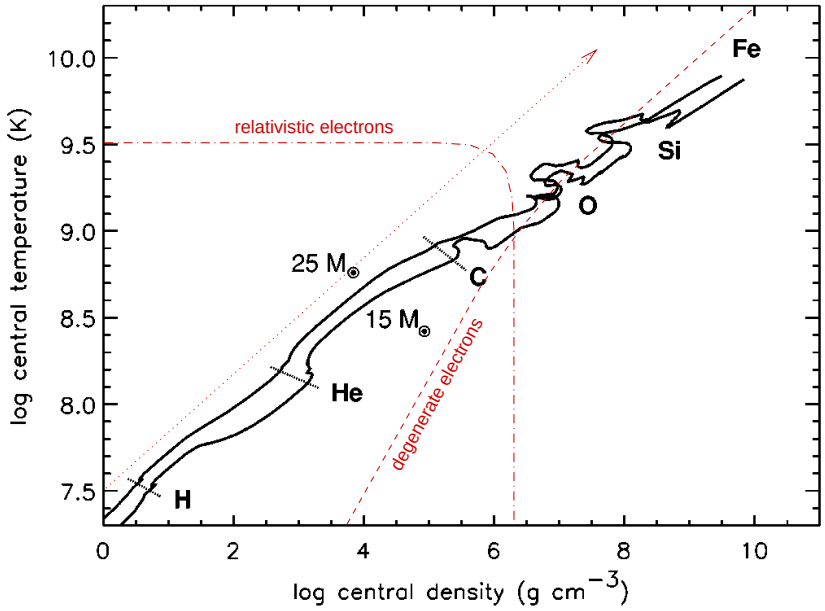

Figure 11.5. Evolution of central temperature and density of 15 $M_\odot$ and 25 $M_\odot$ stars at $Z = 0.02$ through all nuclear burning stages up to iron-core collapse. The dashed line indicated where electrons become degenerate, and the dash-dotted line shows where electrons become relativistic ($\epsilon_e \approx m_e c^2$). The overall evolution trend is an increase of temperature and density roughly following $T_c \propto {\rho_c}^{1/3}$ as expected from homologous contraction in our schematic picture (Chapter 7, shown as a dotted arrow), but some deviation to higher ρ and lower T occurs due to neutrino losses. Non-monotonic (non-homologous) behaviour is seen whenever nuclear fuels are ignited and a convective core is formed. (Figure adapted from Woosley, Heger & Weaver 2002.)

11.3.1 Evolution with significant neutrino losses

Apart from neutrinos produced as a by-product of some nuclear reactions, at high T and ρ several weak interaction processes result in spontaneous neutrino production (see K&W section 18.6 for more details):

- pair annihilation occurs at $T > 10^9$ K: energetic photons can undergo pair creation ($\gamma + \gamma \leftrightarrow e^+ + e^-$), but once in every $\sim 10^{19}$ cases the pair annihilates into neutrinos: $e^+ + e^- \rightarrow \nu + \overline{\nu}$
- photo-neutrino process: this is similar to Compton scattering of a photon off an electron, but there is a small probability that a $\nu\overline{\nu}$ pair is formed instead: $\gamma + e^- \rightarrow e^- + \nu + \overline{\nu}$
- plasma-neutrino process: this involves the decay of a quantized, excited plasma state (a 'plasmon') into $\nu + \overline{\nu}$, and occurs in electron-degenerate gas at high densities ($\rho \gtrsim 10^6$ g/cm^3)
- Bremsstrahlung neutrinos (at low T and very high ρ) are produced by inelastic ("free-free") scattering of an electron in the Coulomb field of a nucleus, producing a $\nu\overline{\nu}$ pair instead of the usual γ photon.

When the central temperature exceeds $\sim 5 \times 10^8$ K, neutrino losses are the most important *energy leak* from the stellar centre, taking away energy much more rapidly than photon diffusion or even convection can transport it to the surface. Therefore $L_\nu \gg L$, so that during nuclear burning $L_{\rm nuc} = \dot{E}_{\rm nuc} \approx L_\nu$ leading to a much shorter nuclear timescale $\tau_{\rm nuc} = E_{\rm nuc}/L_\nu \ll E_{\rm nuc}/L$. Similarly the rate of core contraction (on the thermal timescale) in between burning cycles speeds up: $\dot{E}_{\rm gr} \approx L_\nu$ so that

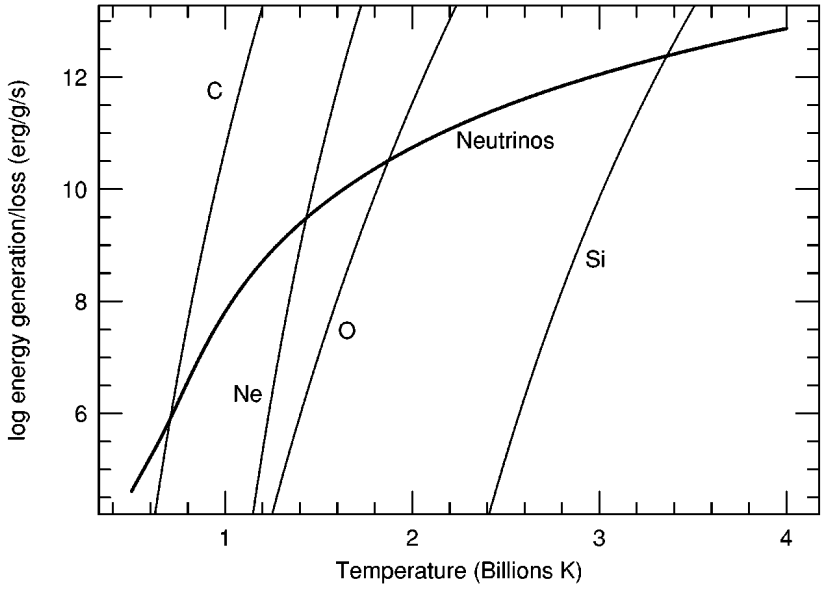

Figure 11.6. Energy generation rate and neutrino loss rate during the advanced evolution of a massive star. The center is assumed to follow a track approximating that shown in Fig. 11.5. The intersections of the nuclear burning lines with the neutrino loss line define the burning temperature of the corresponding fuel. The lifetime of each burning stage is approximately equal to the energy generated by nuclear burning ($\sim 4.0, 1.1, 5.0$ and 1.9×10^{17} erg/g for C-, Ne-, O- and Si-burning respectively) divided by the energy generated per gram and per second at balanced power as defined by the intersections of $\epsilon_{\rm nuc}$ and ϵ_ν. Thus the lifetime ranges from several 10^3 years for C-burning to about a day for Si-burning! (Figure from Woosley, Heger & Weaver 2002.)

$\tau_{\rm th} = E_{\rm gr}/L_\nu \ll E_{\rm gr}/L$. Therefore the rate of evolution speeds up enormously, and accelerates as the core contracts and heats up.

The dependence of nuclear energy generation and neutrino losses on temperature are depicted in Fig. 11.6, for the centre of a massive star. Both ϵ_ν and $\epsilon_{\rm nuc}$ increase strongly with temperature, but the T-dependence of $\epsilon_{\rm nuc}$ is larger than that of ϵ_ν. During nuclear burning cycles energy production and cooling are in balance, $\epsilon_{\rm nuc} = \epsilon_\nu$, and this condition defines the temperature at which burning takes place. Note that nuclear burning in the presence of neutrino losses is stable: a small perturbation $\delta T > 0$ would increase the local heat content ($\epsilon_{\rm nuc} > \epsilon_\nu$), leading to expansion and cooling of the core until thermal equilibrium is re-established.

11.3.2 Advanced nuclear burning cycles: carbon burning and beyond

When the temperature in the contracting CO core reaches $5 - 8 \times 10^8$ K (depending on the mass of the core), carbon is the first nuclear fuel to be ignited. The reactions involved in carbon burning and further nuclear burning cycles were treated in Sect. 5.4.5. In the following sections we briefly review these and discuss the consequences for the structure and evolution of the star. A typical example of the interior evolution is shown in Fig. 11.7 for a 15 $M_\odot$ star.

Carbon burning

Carbon burning proceeds via the ^{12}C + ^{12}C reaction, which produces a mixture of products, mainly ^{20}Ne and some ^{24}Mg. In stars with masses up to about 20 $M_\odot$ the large nuclear luminosity produces a convective core (as shown in Fig. 11.7) of about 0.5 $M_\odot$. On the other hand, in more massive stars carbon burns radiatively, because the initial ^{12}C abundance is smaller and nuclear burning is

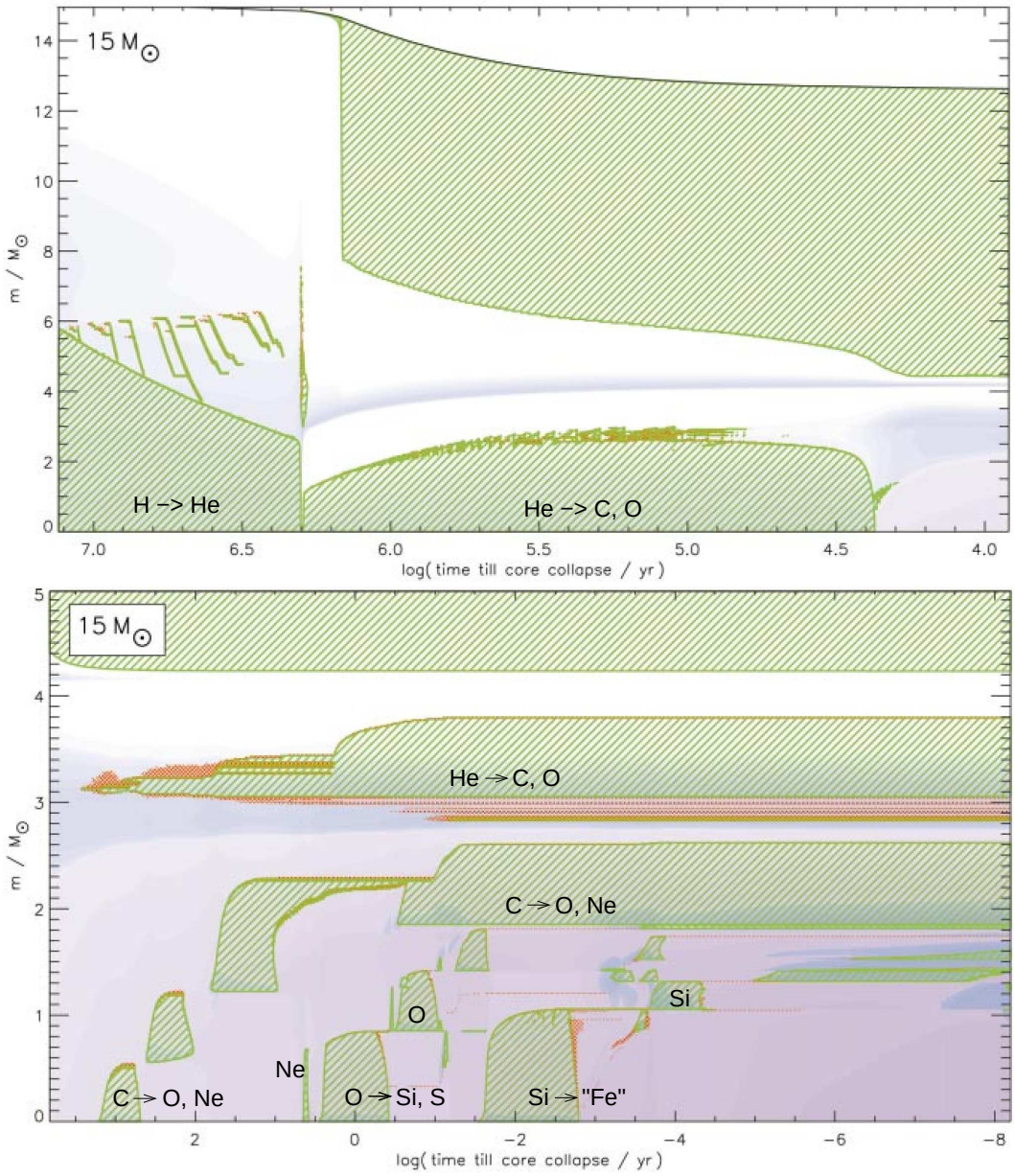

Figure 11.7. Kippenhahn diagram of the evolution of a 15 $M_\odot$ star showing convective regions (cross-hatching) and nuclear burning intensity (blue shading) during central H and He burning (top panel) and during the late stages in the inner 5 $M_\odot$ of the star (bottom panel). A complicated series of convective burning cores and shells appear, due to respectively carbon burning (around $\log t \sim 3$), neon burning (around $\log t \sim 0.6$), oxygen burning (around $\log t \sim 0$) and silicon burning (around $\log t \sim -2$). Figure from Woosley, Heger & Weaver (2002.)

less efficient and photons are able to carry off the small excess energy not emitted in neutrinos. The duration of the C-burning phase is of the order of 10^3 yrs. It should be noted that these results are sensitive to the uncertain rate of the $^{12}C(\alpha,\gamma)^{16}O$ rate, which determines the ^{12}C abundance left after He-burning – a lower rate will leave more ^{12}C to be burned and this increases both the size of the convective core and the duration of the C-burning phase.

Following carbon exhaustion in the centre, the core (now composed mostly of O, Ne and Mg)

Table 11.1. Properties of nuclear burning stages in a 15 $M_\odot$ star (from Woosley et al. 2002).

burning stage	T (10^9 K)	ρ (g/cm^3)	fuel	main products	timescale
hydrogen	0.035	5.8	H	He	1.1×10^7 yr
helium	0.18	1.4×10^3	He	C, O	2.0×10^6 yr
carbon	0.83	2.4×10^5	C	O, Ne	2.0×10^3 yr
neon	1.6	7.2×10^6	Ne	O, Mg	0.7 yr
oxygen	1.9	6.7×10^6	O, Mg	Si, S	2.6 yr
silicon	3.3	4.3×10^7	Si, S	Fe, Ni	18 d

contracts on its (neutrino-accelerated) Kelvin-Helmholtz timescale and carbon burning continues in a convective shell around this core. A number of such convective shell-burning episodes can follow as shown in Fig. 11.7, their number depending on the mass of the star. The discrete nature of these shell burning events can also produce a discrete (discontinuous) dependence of the final state of the core on the initial stellar mass.

In stars with masses up to about 11 $M_\odot$ (CO core masses up to 1.4 $M_\odot$) carbon burning proceeds somewhat differently. The CO core becomes partially degenerate and neutrino losses effectively cool the centre of the star, so that carbon does not ignite in the centre but in an off-centre shell in a mildly degenerate flash (analogous to, but less violent than the He flash in low-mass stars). After one or more of these mild carbon flashes the burning front moves to the centre and stable carbon burning in a convective core follows. After carbon burning, the O-Ne-Mg core becomes degenerate and no further nuclear burning is ignited. The fate of such stars is uncertain and depends on whether the core can reach the Chandrasekhar limit by shell burning (in which case the core eventually collapses, producing a supernova) or whether mass loss is strong enough to remove the envelope, leaving a O-Ne-Mg white dwarf.

Neon and oxygen burning

In stars with masses $\gtrsim 11\ M_\odot$, once the temperature in the contracting O-Ne core reaches $\approx 1.5{\times}10^9$ K neon is 'burned' into oxygen and magnesium by a combination of photo-disintegration and α-capture reactions. Neon burning always occurs in a convective core, regardless of stellar mass. By this time increased neutrino losses have accelerated the rate of evolution by a factor $\sim 10^3$ compared to the carbon-burning phase (see Fig. 11.6). The duration of the neon-burning phase is therefore very short, of order 1 year. Neon burning then shifts to a shell, as was the case for carbon burning, but in this case the time left until the next fuel is ignited is so short that no significant shell burning occurs.

When $T_9 \approx 2.0$ oxygen is ignited in the core by means of the ^{16}O + ^{16}O reaction, producing mostly ^{28}Si and ^{32}S with a significant admixture of other isotopes (see below). Oxygen burning also occurs in a convective core with a typical mass of $\approx 1.0\ M_\odot$ (see Fig. 11.7). The duration is similar to that of neon burning, of order 1 year, despite the higher neutrino loss rate at this stage. (The reasons for this 'long' duration are the large oxygen mass fraction, ~ 0.7, and the large energy gain per gram compared to Ne burning.) Similar to previous burning stages, after central oxygen burning a number of convective oxygen-burning shells appears in quick succession. By this point the remaining time until core collapse (< 1 yr) is so short that the overlying helium- and carbon-burning shells remain frozen into the stellar structure.

Apart from ^{28}Si and ^{32}S, oxygen burning produces several neutron-rich nuclei such as ^{30}Si, ^{35}S and ^{37}Cl. Partly these result from α-captures on n-rich isotopes already present during C-burning, and partly from weak interactions (electron captures) such as ^{30}P(e$^-$, ν)^{30}Si. As a result the overall

number of neutrons in the remnant Si-S core exceeds the number of protons (p/n < 1) and therefore that of electrons (implying that $\mu_e > 2$).

Silicon burning

When the central temperature exceeds 3×10^9 K, a process known as silicon burning starts. Rather than a fusion reaction this is a complex combination of photo-disintegration and α-capture reactions. Most of these reactions are in equilibrium with each other, and their abundances can be described by nuclear equivalents of the Saha equation for ionization equilibrium. For $T > 4 \times 10^9$ K a state close to *nuclear statistical equilibrium* (NSE) can be reached, where the most abundant nuclei are those with the lowest binding energy, i.e. of isotopes belonging to the *iron group*. The abundances are further constrained by the total number of neutrons and protons present. Due to the high neutron content of the oxygen burning ashes (see above), the final composition is mostly ^{56}Fe and ^{52}Cr.

Silicon burning also occurs in a convective core of $\approx 1\,M_\odot$ and its duration is extremely short, of order 10^{-2} yr. As in previous phases, several convective shell-burning episodes usually follow in quick succession. The precise extent and number of these convective events determines the exact value of the final mass of the *iron core*, which has important consequences for the following core collapse and supernova phase (see Sec. 11.4).

Pre-supernova structure

We have obtained the following general picture. After exhaustion of a fuel (e.g. carbon) in the centre, the core contracts and burning continues in a shell around the core. Neutrino losses speed up the contraction and heating of the core, until the next fuel (e.g. neon) is ignited in the centre. At each subsequent burning stage the outer burning shells have advanced outward, while neutrino cooling is more efficient, resulting in a smaller burning core (in mass) than the previous stage. Eventually this leads to an *onion-skin* structure of different layers consisting of heavier nuclei at increasing depth, separated by burning shells (see Fig. 11.8). Often the central and shell burnings drive convective regions that partially mix the various onion-skin layers. This eventually leads to complicated abundance profiles just before the iron core collapses, an example of which is shown in Fig. 11.9 for a 15 $M_\odot$ star.

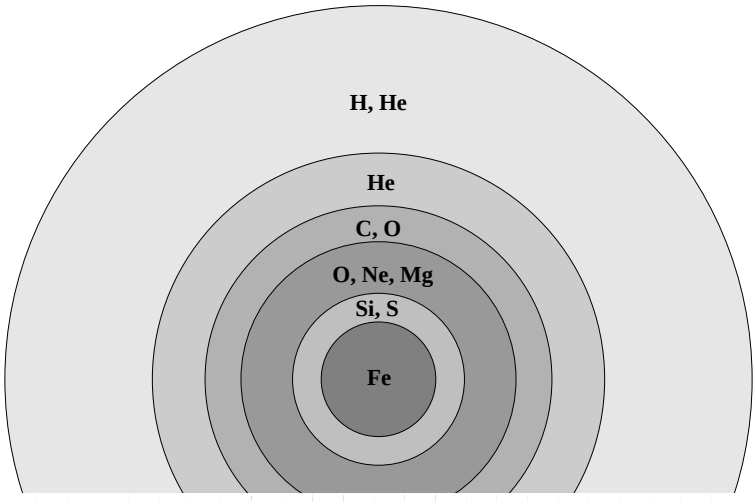

Figure 11.8. Schematic overview of the onion-skin structure of a massive star at the end of its evolution.

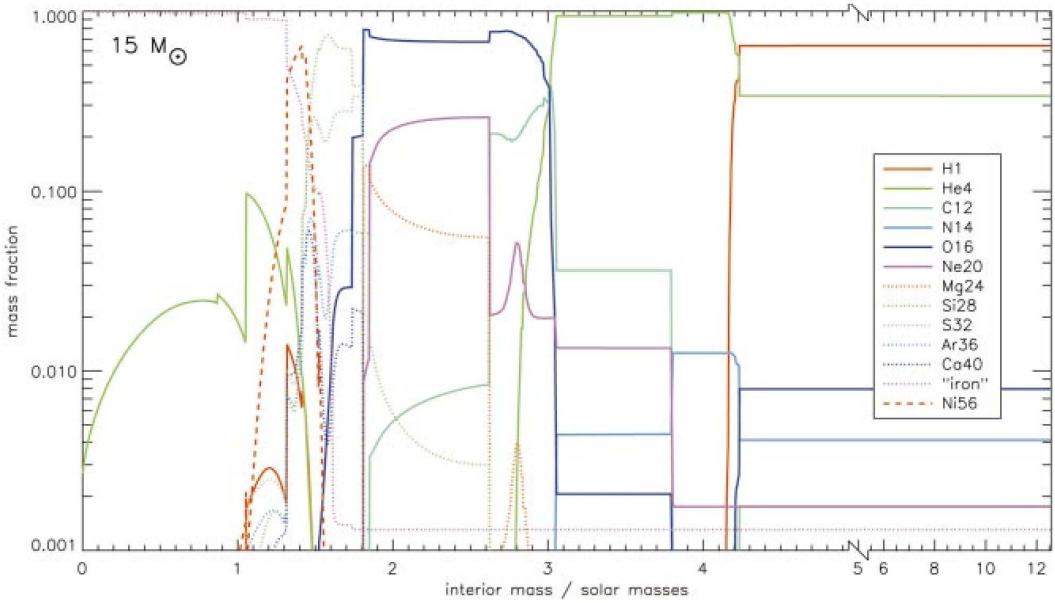

Figure 11.9. Final composition profiles of a 15 $M_\odot$ star (see Fig. 11.7), just before core collapse. "Iron" refers to the sum of neutron-rich nuclei of the iron group, especially ^{56}Fe. (Figure from Woosley, Heger & Weaver 2002.)

11.4 Core collapse of massive stars

At the end of the silicon burning phase, when the central temperature exceeds 4×10^9 K, the composition of the central core is determined by nuclear statistical equilibrium, which means the mixture of nuclei has reached the minimum possible nuclear binding energy at that temperature, i.e. mainly ^{56}Fe. From this iron core no further energy can be extracted by nuclear fusion: it has become inert.

The iron core is in a peculiar state in several respects. Because of neutrino cooling during the late evolution stages, the core typically has a considerable degree of electron degeneracy, except for the largest stellar masses (see Fig. 11.5). However, the high temperature and density ($\gtrsim 10^9$ g/cm^3) mean that the electrons are always relativistic (their typical energy exceeds $m_e c^2$). In that case contraction cannot be stopped, even if the core is degenerate, and must continue on the very rapid, neutrino-mediated thermal timescale. Furthermore, since the relativistic electron gas dominates the pressure, the adiabatic exponent $\gamma_{\rm ad}$ is close to $\frac{4}{3}$. The iron core is therefore very close to a state of dynamical instability. Two processes occur at high density and temperature that contribute to accelerating the (already rapid) contraction into a dynamical collapse of the core.

Electron captures At very high density free electrons can be captured and bound into otherwise β-unstable heavy nuclei. This process, also known as inverse β-decay, occurs when the most energetic electrons have energies high enough to overcome the difference in nuclear binding energy (see also Sec. 10.2). As a result, the composition becomes increasingly neutron-rich – a process known as *neutronization*. Furthermore, the electron pressure decreases which can destroy the precarious state of hydrostatic equilibrium and trigger the collapse of the core.

If the core is significantly degenerate, the Chandrasekhar mass plays an important role. For a composition of predominantly ^{56}Fe one would expect $M_{\rm Ch} = 5.83\,\mu_e^{-2}\,M_\odot \approx 1.26\,M_\odot$. Electron captures increase the average mass per free electron (μ_e) and thus decrease the effective Chandrasekhar mass. This can bring the core mass above this critical mass and facilitate its collapse.

Electron captures can also trigger the collapse of stars with initial masses below $\approx 11\,M_\odot$, which develop degenerate O-Ne-Mg cores at the end of their lives. If the mass of this core can grow (through shell burning) to $1.37\,M_\odot$, electrons are captured by ^{24}Mg and ^{20}Ne which brings about the core to collapse.

Photodisintegration If the temperature in the contracting core reaches values close to 10^{10} K, the energy of the photons becomes large enough to break up the heavy nuclei into lighter ones, in particular ^{56}Fe is disintegrated into α particles and neutrons:

$$^{56}\mathrm{Fe} + \gamma \leftrightarrow 13\,^4\mathrm{He} + 4\,\mathrm{n} \tag{11.4}$$

This reaction is in statistical equilibrium and the abundances of the nuclei involved are determined by a Saha-type equation, the balance shifting more towards the right-hand side the higher the temperature. The process is thus similar to the ionization of hydrogen, and results in lowering $\gamma_{\rm ad}$ to below the critical value of $\frac{4}{3}$. The core therefore becomes dynamically unstable. This process dominates in relatively massive iron cores.

The photodisintegration of ^{56}Fe requires a lot of energy, about 2 MeV per nucleon. This energy is absorbed from the radiation field and thus ultimately from the internal energy of the gas. As a result the pressure decreases quite drastically, triggering an almost free-fall collapse of the core.

The collapse is extremely rapid, taking of the order of 10 msec, because of the short dynamical timescale at the high density ($\sim 10^{10}$ g/cm^3) when the collapse is initiated. During the collapse the temperature and pressure keep rising, but never enough to reverse the collapse until nuclear densities are reached. Further photodisintegrations can occur due to the increasing photon energies, which was once thought (prior to 1980) to dissociate even the α particles completely into free protons and neutrons ($^4\mathrm{He} + \gamma \rightarrow 2\,\mathrm{p} + 2\,\mathrm{n}$, which would require another 7 MeV per nucleon of internal energy from the gas). It has since become clear that full dissociation of ^{56}Fe into α particles and free nucleons does not occur during the collapse. On the other hand, electron captures onto protons ($\mathrm{p} + \mathrm{e}^- \rightarrow \mathrm{n} + \nu$) inside the heavy nuclei continue the process of neutronization, creating more and more neutron-rich nuclei. These eventually merge, creating what is essentially a gigantic stellar-mass nucleus, when ρ approaches nuclear densities of the order 10^{14} g/cm^3. The composition inside the core is predominantly neutrons, which become degenerate and thereby modify the equation of state to suddenly become 'stiff', i.e. the neutron gas becomes almost incompressible. This terminates the collapse at a core radius of $R_{\rm core} \approx 20$ km.

11.4.1 Energetics of core collapse and supernova explosion

The gravitational energy released during the collapse of the core can be estimated as

$$E_{\rm grav} \approx -\frac{GM_{\rm c}^2}{R_{\rm c,i}} + \frac{GM_{\rm c}^2}{R_{\rm c,f}} \approx \frac{GM_{\rm c}^2}{R_{\rm c,f}} \approx 3 \times 10^{53}\,\mathrm{erg}, \tag{11.5}$$

assuming homologous collapse of a core of $M_{\rm c} \approx 1.4\,M_\odot$ from initial radius $R_{\rm c,i} \approx R_{\rm WD}$ to final radius $R_{\rm c,f} \approx 20\,\mathrm{km} \ll R_{\rm c,i}$. Let us compare this with the energy necessary to expel the envelope, which has no time to follow the core collapse,

$$E_{\rm env} = \int_{M_{\rm c}}^{M} \frac{Gm}{r}\,dm \ll \frac{GM^2}{R_{\rm c,i}} \approx 3 \times 10^{52}\,\mathrm{erg} \tag{11.6}$$

for $M = 10\,M_\odot$. Taking into account a realistic mass distribution in the envelope, this estimate comes down to $E_{\rm env} \sim 10^{50}$ erg, so that only a small fraction of the energy released in the collapse of the core is needed to blow away the envelope. The question is therefore how such a small fraction of the collapse energy can be transformed into kinetic energy of the envelope.

When the inner part of the core is compressed to ~ 1.5 times nuclear density, it bounces back like a spring – an event named *core bounce*. As the velocity of the inner core material is reversed, it encounters matter from the still free-falling outer part of the core. If the collision were perfectly elastic, the outer core would bounce back to its initial radius even if the inner core were stationary. The outward motion of the inner core thus gives the possibility of a 'super-elastic' core bounce that might conceivably explode the star. The impact of the infalling matter is supersonic and creates a shock wave that steepens as it travels outward into regions of lower density. The kinetic energy stored in the shock wave was once thought to be sufficient to blow off the envelope, giving rise to a so-called *prompt explosion*. However, two problems arise that prevent such a prompt explosion to occur.

First, as the shock wave travels through the infalling matter which still mostly consists of iron-group nuclei, it heats up the nuclei and disintegrates them effectively into protons and neutrons. We can estimate the energy spent in photodisintegration by noting that the binding energy of an ^{56}Fe nucleus is about 9 MeV/nucleon, so that the disintegration of an iron core of $1.4\,M_\odot$ (1.7×10^{57} nucleons) requires about 2×10^{52} erg. Note that this amounts to absorbing, during a fraction of a second, practically all of the nuclear energy that was released during the lifetime of the star!

Second, electron captures on the free protons created behind the shock produce energetic neutrinos. These neutrinos take away the largest fraction of the energy released in the collapse, especially as the shock moves into relatively low-density regions ($< 10^{12}$ g/cm^3) from where they can easily escape. In the case of supernova 1987A these neutrinos have been detected (see Chapter 12). As a result, the shock wave fizzles out before it reaches the envelope of the star and no prompt explosion occurs.

11.4.2 Effects of neutrinos

The role played by neutrinos during core collapse requires closer examination. The neutrinos produced *before* the collapse set in had typical energies of the order of the thermal energy of the electrons (see Sect. 11.3.1). During the collapse neutrino production by neutronization (inverse β-decay) dominates. The typical energy of these neutrinos is of the order of the Fermi energy of the relativistic electrons,

$$\frac{E_\nu}{m_{\rm e}c^2} \approx \frac{E_{\rm F}}{m_{\rm e}c^2} = \frac{p_{\rm F}}{m_{\rm e}c} = \frac{h}{m_{\rm e}c}\left(\frac{3}{8\pi}\,\frac{\rho}{\mu_{\rm e}m_{\rm u}}\right)^{1/3} \approx 10^{-2}\left(\frac{\rho}{\mu_{\rm e}}\right)^{1/3}, \tag{11.7}$$

using eq. (3.33) and the relation $\rho = \mu_{\rm e} m_{\rm u} n_{\rm e}$, and with ρ in g/cm^3 in the last equality. In the presence of heavy nuclei, the neutrinos interact mainly through so-called coherent scattering with these nuclei, with a typical cross section of the order

$$\sigma_\nu \approx 10^{-45}\,A^2\left(\frac{E_\nu}{m_{\rm e}c^2}\right)^2 \text{cm}^2, \tag{11.8}$$

which gives together with eq. (11.7),

$$\sigma_\nu \approx 10^{-49}\,A^2\left(\frac{\rho}{\mu_{\rm e}}\right)^{2/3} \text{cm}^2. \tag{11.9}$$

If $n = \rho/(Am_{\rm u})$ is the number density of nuclei, the mean free path ℓ_ν of the neutrinos in the collapsing core can then be estimated as

$$\ell_\nu \approx \frac{1}{n\sigma_\nu} \approx 2\times10^{25}\,\frac{1}{\mu_{\rm e}A}\left(\frac{\rho}{\mu_{\rm e}}\right)^{-5/3}\ {\rm cm}. \tag{11.10}$$

Taking $\mu_{\rm e} \approx 2$ and $A \approx 100$, we find with eq. (11.10 that $\ell_\nu \approx 10^7$ cm (the typical dimension of the collapsing core) when $\rho/\mu_{\rm e} \approx 4\times10^9$ g/cm^3. Apparently, neutrinos can no longer escape freely at the high densities prevailing in the collapsing core. The core becomes opaque for neutrinos, which can only diffuse out of the core via many scattering events. Towards the end of the collapse phase, when $\rho > 3\times10^{11}$ g/cm^3, the diffusion velocity even becomes smaller than the infall velocity of the gas, so that neutrinos are *trapped* in the core. Analogous to the photosphere of a star, one can define a 'neutrinosphere' in the outer layers of the core where the density is low enough for the neutrinos to escape. Interior to this, there is a 'neutrino trapping surface' below which the neutrinos are trapped.

The real situation is much more complicated because σ_ν depends on the neutrino energy, so that the neutrino transport problem has to be solved in an energy-dependent way. The congestion of neutrinos in the core causes them to become degenerate (since neutrinos are fermions) with a high Fermi energy. Electron capture becomes less probable, because the new neutrinos have to be raised to the top of the Fermi sea. Neutronization therefore effectively stops when $\rho \approx 3\times10^{12}$ g/cm^3. Only after some neutrinos have diffused out of the core can further neutronization take place. The process of neutronization therefore takes several seconds, while the collapse only takes a few milliseconds.

The deposition of neutrino energy in the core provides an energy source that may revive the shock wave and cause an explosion. Neutrinos diffusing out of the dense core heat the region through which the former shock wave has passed and cause it to become convectively unstable. Convection thus provides a way to convert some of the thermal energy from neutrino deposition into kinetic energy. Multi-dimensional hydrodynamical calculations show that the outward force thus created can overcome the ram pressure of the outer layers that are still falling onto the core and launch a successful explosion, but only for rather low initial stellar masses (up to $\sim 11\,M_\odot$). Alternative ways of reviving the shock and driving a successful supernova explosion are still being explored.

Suggestions for further reading

The evolution of massive stars, including the effects of mass loss and rotation, is treated in detail in Chapters 27 and 28.1-4 of Maeder. A thorough review of the current state of our understanding of the evolution of massive stars, their explosions and nucleosynthesis is given by Woosley, Heger & Weaver (2002, Rev. Mod. Ph., 74, 1015). Several of the figures from this article are reproduced in this chapter.

Exercises

11.1 Mass loss of massive stars during the main sequence

The mass-luminosity relation for massive stars on the main sequence is approximately

$$\log\left(\frac{L_*}{L_\odot}\right) \approx 0.781 + 2.760\times\log\left(\frac{M_i}{M_\odot}\right),$$

where M_i is the initial mass. The mass loss rate of massive stars can roughly be approximated by

$$\log \dot{M} \approx -12.76 + 1.3 \times \log\left(\frac{L_*}{L_\odot}\right).$$

The duration of the main sequence phase $\tau_{\rm MS}$ in years is approximately

$$\log \tau_{\rm MS} \approx 7.719 - 0.655 \times \log\left(\frac{M_i}{M_\odot}\right).$$

(a) Calculate the fraction of mass that is lost by massive stars with $M_i = 25, 40, 60, 85$ and $120\ M_\odot$ during the main sequence phase.

(b) A star with an initial mass of $85\ M_\odot$ on the zero age main sequence has a convective core that contains 83 % of the mass. Calculate the time at which products of nuclear burning will appear at the surface.

(c) *Wolf-Rayet* (WR) stars are massive stars that have lost practically their complete hydrogen rich envelope. They can be classified according to their surface abundances:

WC No hydrogen, high abundances of He, C and O

WNE No Hydrogen, N/He ratio consistent with CNO equilibrium

WNL Some Hydrogen, N/He ratio consistent with CNO equilibrium

Put the sub-classifications in 'chronological order'. What type of WR is the star in question b)?

11.2 Maximum mass loss rate for a radiation driven wind

(a) Assume that all photons transfer their entire *momentum* to the outflowing wind[3]. Show that the maximum mass loss rate that can be driven by radiation is given by

$$\dot{M} < \dot{M}_{\rm max} = \frac{L}{v_\infty c},$$

where v_∞ is the velocity of the wind at a large distance of the star.

(b) Show that with this maximum mass loss rate, the *kinetic energy* of the wind is only a small fraction of the luminosity, i.e.

$$\frac{1}{2}\dot{M}_{\rm max} v_\infty^2 \ll L \quad (v_\infty \approx 3 v_{\rm esc})$$

11.3 Burning stages

(a) Explain why the timescales of the burning stages from C-burning onward are very short compared to the H- and He-burning phases.

(b) Why does neon burning precede oxygen burning (why does it occur at a lower temperature) even though ^{20}Ne is a heavier nucleus than ^{16}O?

(c) The end result of nuclear burning in a massive star is an onion-like structure of the ashes of the various nuclear burning stages. Try to identify these layers, and the nuclear reactions that are responsible for them, in Figure 11.9.

[3]Under certain circumstances a photon can transfer its momentum more than one time. Can you imagine how? We suspect that this effect is important in the stellar winds of Wolf Rayet stars.